



1 **High Resolution Tropospheric Carbon Monoxide Profiles**
2 **Retrieved from CrIS and TROPOMI**

3

4 **Dejian Fu¹, Kevin W. Bowman¹, Helen M. Worden², Vijay Natraj¹, John R.**
5 **Worden¹, Shanshan Yu¹, Pepijn Veefkind^{3,4}, Ilse Aben⁵, Jochen Landgraf⁵,**
6 **Lawrence Strow⁶, Yong Han⁷**

7 [1]{NASA Jet Propulsion Laboratory, California Institute of Technology, Pasadena,
8 California, United States of America}

9 [2]{National Center for Atmospheric Research, Boulder, Colorado, United States of
10 America}

11 [3]{Royal Netherlands Meteorological Institute, Utrechtseweg, De Bilt, The Netherlands}

12 [4]{Delft University of Technology, Department of Geoscience and Remote Sensing,
13 Stevinweg 1, Delft, The Netherlands}

14 [5]{SRON Netherlands Institute for Space Research, Sorbonnelaan, Utrecht, The
15 Netherlands}

16 [6]{University of Maryland, Baltimore, Maryland, United States of America}

17 [7]{Center for Satellite Applications and Research, National Environmental Satellite, Data,
18 and Information Service, NOAA, College Park, Maryland, United States of America}

19 Correspondence to: Dejian Fu (dejian.fu@jpl.nasa.gov)

20

21 **Abstract**

22 The Measurements of Pollution in the Troposphere (MOPITT) instrument is the only satellite-
23 borne sensor in operation that uses both thermal (TIR) and near infrared (NIR) channels to
24 estimate CO profiles. With more than fifteen years (2000 to present) of validated multi-
25 spectral observations, this air quality and climate record provides the unique capability to
26 separate CO in the Lower Most Troposphere (LMT, surface to 3 km (~700 hPa)) from the free
27 tropospheric abundance. To extend this record, a new, hyper-spectral approach is presented
28 here that will provide CO data products exceeding the capabilities of MOPITT instrument by



1 combining the short wavelength infrared (SWIR, equivalent to the MOPITT NIR) channels
2 from The TROPOspheric Monitoring Instrument (TROPOMI) aboard the European Sentinel 5
3 Precursor (S5p) satellite, and the TIR channels from the Cross-track Infrared Sounder (CrIS)
4 aboard Suomi National Polar-orbiting Partnership (Suomi NPP) satellite. We apply the MUlTi-
5 SpEctra, MUlTi-SpECies, MUlTi-SENSors (MUSES) retrieval algorithm, to quantify the
6 potential of this joint CO product. CO profiles are retrieved from a single-footprint, full
7 spectral resolution CrIS transect over Africa on August 27-28, 2013 coincident with
8 significant biomass burning. Comparisons of collocated CrIS and MOPITT CO observations
9 for the LMT show a mean difference of 2.8 ± 24.9 ppb, which is well within the estimated
10 measurement uncertainty of both sensors. The estimated degrees of freedom (DOFS) for CO
11 signals from synergistic CrIS/TROPOMI retrievals are 0.9 in the LMT and 1.3 above LMT,
12 which indicates that the LMT CO can be distinguished near surface CO abundance
13 information from the free troposphere, similar to MOPITT multiple spectral observations (0.8
14 in the LMT, and 1.1 above LMT). In addition to increased sensitivity, the combined retrievals
15 reduce measurement uncertainty with $\sim 15\%$ error reduction in LMT. With a daily global
16 coverage and a combined spatial footprint of 14 km, the joint CrIS/TROPOMI measurements
17 have the potential to extend and improve upon the MOPITT multi-spectral CO data records
18 for the coming decade.

19

20 **1 Introduction**

21 Observations of tropospheric carbon monoxide (CO) from space over the last decade have
22 been exploited for monitoring air quality (e.g., Clerbaux et al., 2008; Kar et al., 2010),
23 quantifying CO emissions (e.g., Kopacz et al., 2009; Fortems-Cheiney et al., 2011), analyzing
24 long-range transport of pollution (e.g., Heald et al., 2003; Edwards et al., 2006; Zhang et al.,
25 2006), attributing sources and sinks of CO₂ concentrations (e.g., Silva et al., 2013), and
26 evaluating chemical transport models and decadal trends in atmospheric composition (e.g.,
27 Shindell et al., 2006; Worden et al., 2013a). The Measurements Of Pollution In The
28 Troposphere (MOPITT) instrument, which is on the Earth Observation System EOS-Terra
29 platform, has acquired more than fifteen years (2000 to present) of validated global CO
30 observations (Emmons et al., 2007, 2009; Deeter et al., 2013, 2014). MOPITT is equipped
31 with gas filter correlation radiometers (Drummond, 1992) measuring both CO first
32 fundamental (4.6 μm) and overtone bands (2.3 μm). The synergy of CO first fundamental



1 band in the thermal infrared (TIR) and overtone band in the near infrared (NIR) provides an
2 unprecedented sensitivity to probe CO in the lowermost troposphere (LMT, surface to 3 km)
3 (Worden et al., 2010; Worden et al., 2013b). This unique multi-spectral capability of
4 MOPITT is not available from any single sensor on existing satellites that depend on a single
5 spectral band, e.g., AIRS (Atmospheric Infrared Sounder) on EOS-Aqua (McMillan et al.,
6 2005; Warner et al., 2007), TES (Tropospheric Emission Spectrometer) on EOS-Aura
7 (Rinsland et al., 2006), IASI (Infrared Atmospheric Sounding Interferometer) on METOP-
8 A/B (George et al., 2009), SCIAMACHY on Envisat (de Laat et al., 2007). Retrieval
9 sensitivity to the LMT is critical for the operational use of satellite data in air quality, climate,
10 and carbon applications, motivating the multi-spectral retrieval approach for a variety of
11 species including CO (Landgraf and Hasekamp 2007; Worden et al., 2010; Cuesta et al.,
12 2013; Fu et al., 2013; Worden et al., 2013a, 2013b).

13 All NASA space missions capable of measuring atmospheric CO concentrations have passed
14 their nominal lifetime by years (Table 1). The European Space Agency (ESA) Sentinel 5
15 precursor (S5p) TROPOspheric Monitoring Instrument (TROPOMI), which is expected to
16 launch in 2016 into an afternoon orbit behind the Suomi National Polar-orbiting Partnership
17 (Suomi-NPP) satellite, has only NIR channels for CO measurements. The Cross-track
18 Infrared Sounder (CrIS) aboard the Suomi-NPP satellite is a TIR sensor operating since
19 October 28, 2011 and providing observations at full spectral resolution since December 4,
20 2014. The constellation of Suomi NPP and ESA S5p provides a unique set of collocated
21 observations, which could extend the EOS-MOPITT multi-spectral CO data products with
22 significant improvements on spatial resolution and coverage (Table 1). Joint CrIS/TROPOMI
23 retrieval algorithm can also be applied to the future joint Sentinel-5 UVNS/IASI-NG
24 observations from METOP Second Generation satellites (Veefkind et al., 2012; Crevoisier et
25 al., 2014), which could provide joint TIR/NIR CO measurements in the time period of 2022-
26 2045.

27 In this paper, we describe the MUlti-SpEctra, MUlti-SpEcies, Multi-SENSors (MUSES)
28 retrieval algorithm that combines the TROPOMI and CrIS spectral radiances to produce
29 atmospheric CO Volume Mixing Ratio (VMR) profiles with a vertical resolution that
30 improves upon the EOS-Terra MOPITT multi-spectral CO data products. This multi-spectral
31 observation strategy offers two significant advantages relative to traditional single band



1 measurements: enhanced sensitivity to composition changes especially in the LMT, and
2 reduced measurement uncertainty.

3 The paper is organized as follows: Section 2 describes the characteristics of CrIS/TROPOMI
4 measurements and the pairing strategy. Section 3 describes the MUSES retrieval algorithm,
5 samples of retrievals using CrIS full spectral resolution, single-footprint measurements,
6 comparisons of collocated CrIS and MOPITT observations and estimated characteristics of
7 synergistic CrIS/TROPOMI retrievals. Conclusions are presented in Section 4.

8

9 **2 CrIS and TROPOMI**

10 CrIS is on the Suomi NPP satellite in a near-polar, sun-synchronous, 828 km altitude orbit
11 with a 1:30 pm equator crossing time (ascending node), and has been operational since
12 October 28, 2011. TROPOMI will be on the ESA S5p satellite, planned for launch in summer
13 2016 with a design lifetime of 7 years (Table 1). S5p will fly within approximately 5 minutes
14 of Suomi NPP, which enables collocated observations of atmospheric composition (cloud,
15 aerosol, temperature, and trace gases) and surface properties (albedo, emissivity, and skin
16 temperature), thus building upon the success of the “A-Train” constellation of Earth
17 observation satellites.

18 CrIS is a Fourier transform spectrometer that measures the TIR radiances emitted by the
19 Earth's surface and transmitted through atmospheric gases and particles in three spectral
20 bands, including the long-wave IR band 1 (648.750-1096.250 cm^{-1}), the mid-wave IR band 2
21 (1208.750-1751.250 cm^{-1}), and the short-wave IR band 3 (2153.750-2551.250 cm^{-1}) (Han et
22 al., 2013, 2015; Strow et al., 2013a,b; Tobin et al., 2013; Wang et al., 2013). It was intended
23 as the operational successor to the AIRS instrument on the Aqua Platform (Aumann et al.,
24 2003; Pagano et al., 2003). The typical signal to noise ratio (SNR) of a CrIS measurement is
25 about 800:1 in the spectral region of interest for CO. CrIS is a cross-track scanning
26 instrument, whose full spectral resolution is 0.625 cm^{-1} , providing measurements with daily
27 global coverage (Table 1). Currently, the operational Level 1B products provide full spectral
28 resolution only for the long-wave IR band 1 for entire lifetime of the mission. The full
29 resolution (0.650 cm^{-1}) spectral radiance products for band 2 (was 1.250 cm^{-1}) and band 3
30 (was 2.500 cm^{-1}) have been available since December 4th, 2014. Ground pixels have a
31 diameter of 14.0 km at nadir. CrIS atmospheric measurements in the 2155-2209 cm^{-1} spectral
32 region – nearly identical to observations of MOPITT TIR channels – include high-density



1 absorption features of the strongest fundamental band of CO and minor absorption from
2 interfering species, providing sensitivity for estimating the atmospheric CO concentration. It
3 is worth noting that Gambacorta et al., [2014] found that the information content present in
4 the CO retrievals improves up to one order of magnitude upon switching from spectral
5 resolution of 2.5 cm^{-1} to the full spectral resolution of 0.625 cm^{-1} (starting from December 4th
6 2014).

7 TROPOMI will provide daily global coverage owing to its wide swath across track (Table 1).
8 It is a nadir-viewing push broom imaging spectrometer that measures backscattered and
9 reflected sunlight covering the 270-500 nm, 675-725 nm, 725-775 nm, and 2305-2385 nm
10 ($4193\text{-}4338 \text{ cm}^{-1}$) spectral regions. Its atmospheric measurements in the $2.3 \mu\text{m}$ band – nearly
11 identical to observations of NIR channels of SCIAMACHY and MOPITT – include high-
12 density absorption features of the overtone band of CO, providing sensitivity for estimating
13 the CO total column average VMR. The module of the spectral band at $2.3 \mu\text{m}$ has a spectral
14 resolution of 0.25 nm and a spectral sampling rate of about 2.0-2.5 detector elements per
15 FWHM (Full Width at Half Maximum) (Veefkind et al., 2012). The ground pixel size of its
16 CO measurements at the nadir position is $7 \times 7 \text{ km}^2$, which yields a spatial resolution about 10
17 times higher than Terra-MOPITT ($22 \times 22 \text{ km}^2$) mission (Table 1). Within the spectral region
18 of interest, the minimum spectral SNR of a single TROPOMI measurement is 120:1 in the
19 continuum around 2310 nm (4329 cm^{-1}), specified for a scene with a surface albedo of 5%
20 and solar zenith angle of 70° (Veefkind et al., 2012).

21 In order to match the CrIS footprint size, our retrieval algorithm will average 4 adjacent pixels
22 of TROPOMI prior to the spectral fittings. Hence, the effective SNR of TROPOMI
23 measurements for the synergistic retrievals will be greater than 240:1. The joint
24 CrIS/TROPOMI spatial resolution will be $14 \times 14 \text{ km}^2$ at the nadir position, about 2.5 times
25 higher than that of the MOPITT mission (Table 1).

26 Daytime ascending node CO retrievals are available from TROPOMI and CrIS whereas
27 nocturnal descending node CO depends exclusively on CrIS. The daily spatial sampling of the
28 joint CrIS/TROPOMI measurements is more than 8.0 times better than that of Terra MOPITT
29 since CrIS/TROPOMI measurements have ~ 4 times wider swath and 2.5 times finer ground
30 pixel size compared to MOPITT (Table 1). After performing the temporal and spatial matches
31 among CrIS/TROPOMI measurements, the distances between matched CrIS/TROPOMI
32 observations in the nadir direction are within 3 km – smaller than the pixel sizes of both



1 instruments. The associated temporal differences are within 5 minutes. In general, these
 2 spatial and temporal separations are small compared to the scales of variability anticipated for
 3 CO and could be neglected. Over complex source regions, such as urban areas, the special
 4 treatments on achieving perfect spatial match might be necessary.

5

6 **3 Retrieval algorithm, sample results and retrieval characteristics**

7 This section describes the MUSES algorithm for synergistic retrievals of CO profiles (Section
 8 3.1), sample retrievals when only using CrIS measurements (Section 3.2), synthetic joint
 9 CrIS/TROPOMI CO retrievals to access the characteristics of improved tropospheric CO
 10 profiling when combining TIR/NIR observations (Section 3.3).

11 **3.1 MUSES retrieval algorithm for producing joint TROPOMI and CrIS carbon 12 monoxide volume mixing matrix profile data products**

13 The MUSES retrieval algorithm is based upon Optimal Estimation (OE) method (Rodgers
 14 2000). OE combines a priori knowledge, which includes both a mean state and covariance of
 15 the atmospheric state, and the measurements to infer the atmospheric state. The OE algorithm
 16 computes the best estimate state vector $\hat{\mathbf{x}}$, which represents the concentration of atmospheric
 17 trace gases and ancillary parameters, by minimizing the following cost function

$$18 \quad C(\mathbf{x}) = \|\mathbf{x} - \mathbf{x}_a\|_{\mathbf{S}_a^{-1}}^2 + \|\mathbf{L}_{\text{obs}} - \mathbf{L}_{\text{sim}}(\mathbf{x})\|_{\mathbf{S}_\epsilon^{-1}}^2 \quad (1)$$

19 Equation 1 is a sum of quadratic functions representing Euclidean \mathbf{L}^2 norm ($\|\mathbf{b}\|_{\mathbf{A}}^2 = \mathbf{b}^T \mathbf{A} \mathbf{b}$),
 20 with the first term accounting for the difference between the retrieved vector \mathbf{x} and a priori
 21 state \mathbf{x}_a , inversely weighted by the a priori matrix \mathbf{S}_a , and with the second term representing
 22 the difference between the observed \mathbf{L}_{obs} and simulated $\mathbf{L}_{\text{sim}}(\mathbf{x})$ radiance spectra inversely
 23 weighted by the measurement error covariance matrix \mathbf{S}_ϵ .

24 Under the assumption that measurement error between TROPOMI and CrIS are uncorrelated,
 25 Eq. 1 can be written as:

$$26 \quad C(\mathbf{x}) = \|\mathbf{x} - \mathbf{x}_a\|_{\mathbf{S}_a^{-1}}^2 + \underbrace{\|\mathbf{L}_{\text{obs_TROPOMI}} - \mathbf{L}_{\text{sim_TROPOMI}}(\mathbf{x})\|_{\mathbf{S}_{\epsilon_TROPOMI}^{-1}}^2}_{\text{TROPOMI}} \\
 + \underbrace{\|\mathbf{L}_{\text{obs_CrIS}} - \mathbf{L}_{\text{sim_CrIS}}(\mathbf{x})\|_{\mathbf{S}_{\epsilon_CrIS}^{-1}}^2}_{\text{CrIS}} \quad (2)$$



1 The joint retrieval algorithm iteratively updates the state vector based upon a trust-region
 2 Levenberg-Marquardt optimization algorithm to minimize the cost function in Eq. 2 (Rogers
 3 2000; Bowman et al., 2006):

$$\begin{aligned}
 \mathbf{x}_{i+1} = \mathbf{x}_i + & \left[\mathbf{S}_a^{-1} + \underbrace{\mathbf{K}_{\text{TROPOMI}}^T \mathbf{S}_{\epsilon, \text{TROPOMI}}^{-1} \mathbf{K}_{\text{TROPOMI}}}_{\text{TROPOMI}} + \underbrace{\mathbf{K}_{\text{CrIS}}^T \mathbf{S}_{\epsilon, \text{CrIS}}^{-1} \mathbf{K}_{\text{CrIS}}}_{\text{CrIS}} \right]^{-1} \\
 & * \left[\mathbf{S}_a^{-1} (\mathbf{x}_a - \mathbf{x}_i) + \underbrace{\mathbf{K}_{\text{TROPOMI}}^T \mathbf{S}_{\epsilon, \text{TROPOMI}}^{-1} \Delta \mathbf{L}_{\text{TROPOMI}}}_{\text{TROPOMI}} + \underbrace{\mathbf{K}_{\text{CrIS}}^T \mathbf{S}_{\epsilon, \text{CrIS}}^{-1} \Delta \mathbf{L}_{\text{CrIS}}}_{\text{CrIS}} \right] \quad (3)
 \end{aligned}$$

5 where, \mathbf{K} is the Jacobian matrix representing sensitivity of spectral radiances to the
 6 atmospheric state; and $\Delta \mathbf{L}$ is the difference between observed and simulated spectral
 7 radiances.

8 To simulate thermal infrared spectral radiances $\mathbf{L}_{\text{sim, CrIS}}$ and Jacobians \mathbf{K}_{CrIS} , the joint
 9 TROPOMI and CrIS algorithm incorporates the forward model of TES operational algorithm
 10 (Bowman et al., 2006, Clough et al., 2006), with CrIS specifications (spectral range,
 11 resolution, SNRs, and viewing geometry) obtained from CrIS L1B data products. In the NIR
 12 region, we use the Vector Linearized Discrete Ordinate Radiative Transfer (VLIDORT)
 13 model (Spurr, 2006, 2008), with the specification for TROPOMI measurements (spectral
 14 range, resolution, SNRs) described in Veefkind (2012), to compute the spectral radiances
 15 $\mathbf{L}_{\text{sim, TROPOMI}}$ and Jacobians $\mathbf{K}_{\text{TROPOMI}}$. The characteristics of joint CrIS/TROPOMI CO
 16 retrievals will be illustrated in section 3.3.

17 The joint TROPOMI and CrIS retrievals start with the list of the fitting parameters, a priori
 18 values and a priori uncertainty shown in Table 2. In addition to the initial guess for the trace
 19 gas concentration (CO, H₂O, CH₄, and N₂O), the initial guess for auxiliary parameters used in
 20 the simulation of CrIS radiances (including temperature profile, surface temperature and
 21 emissivity, cloud extinction and top pressure) are also retrieved from CrIS radiances in order
 22 to take into account their spectral signatures in the CO spectral regions.

23 The tandem orbit of Suomi NPP and S5p enables access to the high spatial resolution cloud
 24 information measured by sensors aboard Suomi NPP. This convoy enables cloud-
 25 prescreening using Visible Infrared Imaging Radiometer Suite (VIIRS) cloud products
 26 (Platnick et al., 2013), which is a scanning radiometer on the Suomi NPP satellite. This cloud
 27 prescreening improves the efficiency of data processing and the quality of the retrieved



1 profiles. Cloudy scenes for the CrIS geometry (~14.0 km diameter at nadir) will be
2 characterized using the mature infrared cloud forward modeling techniques used in the TES
3 retrievals (Kulawik et al., 2006; Eldering et al., 2008). For the cloud and aerosol radiative
4 modeling within the Field Of View (FOV) of the TROPOMI sensor, we will adopt the
5 algorithm that has been used in the production of Orbiting Carbon Observatory 2 (OCO-2)
6 version 6 Level 2 standard products (Boesch et al., 2015). We will retrieve the Gaussian
7 parameters that represent the optical depth profiles for water/ice clouds and top two aerosols
8 specified by the Modern Era Retrospective analysis for Research and Applications aerosol
9 reanalysis (MERRAero) climatology (2009-2010) (Table 2). We will use VIIRS Level 2
10 products of surface temperature (Hook et al., 2012), and cloud property (cloud fraction, cloud
11 optical thickness, and cloud top pressure (Baker 2011a,b; 2012)) as a priori information to
12 retrieve ancillary parameters.

13 Optimal estimation theory provides a tool to enable estimation of the characteristics e.g.,
14 vertical resolution/sensitivity and uncertainty of measurements, and was applied to evaluating
15 the characteristics of Aura TES (Bowman et al., 2006), joint TES/OMI data products (Fu et
16 al., 2013), and MOPITT data products (Worden et al., 2010). The averaging kernel matrix (**A**)
17 and error covariance (**S**) of CO profiles, can be calculated using the following equations
18 (Rodgers, 2000),

$$19 \quad \mathbf{A} = \mathbf{G}\mathbf{K} \quad (4)$$

20 and

$$21 \quad \mathbf{S} = (\mathbf{I} - \mathbf{A})\mathbf{S}_a(\mathbf{I} - \mathbf{A})^T + \mathbf{G}\mathbf{S}_\epsilon\mathbf{G}^T \quad (5)$$

22 Where, **I** is the unitary matrix, **S_a** is the a priori covariance matrix of retrieved state, **S_ε** is the
23 measurement noise covariance, and **G**, the gain matrix, can be written as the following
24 equation,

$$25 \quad \mathbf{G} = (\mathbf{K}^T\mathbf{S}_\epsilon^{-1}\mathbf{K} + \mathbf{S}_a^{-1})^{-1}\mathbf{K}^T\mathbf{S}_\epsilon^{-1} \quad (6)$$

26

27 **3.2 Carbon monoxide measured from CrIS and MOPITT during an African** 28 **biomass burning event**

29 A biomass-burning event is observed in Aqua MODIS fire data products (Giglio et al., 2003;
30 Davies et al., 2004), collocated with the CrIS and MOPITT ground tracks, on August 27th,



1 28th 2014 over Africa (Fig. 1). The CO concentration in the LMT during this biomass-burning
2 event shows a strong latitudinal gradient with local variation, based on the MOPITT
3 observations. This gradient provides an excellent opportunity to evaluate the performance of
4 CrIS and future CrIS/TROPOMI retrievals (section 3.3). We applied the MUSES algorithm to
5 retrieve CO profiles using real CrIS full spectral resolution, single footprint measurements,
6 and then compared the retrieved profiles to the collocated MOPITT observations. When
7 running in the retrieval mode that only uses CrIS measurements, the TROPOMI terms in the
8 right-hand side of Eq. 2 and Eq. 3 vanish.

9 The CrIS measurements clearly capture the CO gradient centered at 10°S and diminishing
10 poleward to roughly 20°S (Figs. 2 and 3), associated with the biomass-burning event detected
11 by the enhanced MODIS radiative fire power (Fig. 1). Table 3 shows the mean and RMS of
12 the difference between CrIS and MOPITT TIR CO observations in LMT is -6.9 ± 22.8 ppb,
13 respectively, which is better than the differences between CrIS and MOPITT multi-spectral
14 observations (-22.9 ± 38.8 ppb, Table 3). The differences between CrIS and MOPITT observed
15 CO VMR could arise from the following three sources: [1] a priori CO profiles used in the
16 retrievals (Figs 2D, 2E; Fig. 3B); [2] measurement sensitivity; [3] measurement date/time
17 (MOPITT local time 10:30 am on August 27th, CrIS local time 1:30 pm on August 28th,
18 2013).

19 The diurnal variation of MODIS fire radiative power and fire counts for the time period of
20 August 27 to 28, 2013, is weak. In order to evaluate the impacts of the sources [1] and [2], the
21 retrievals for the same set of soundings were recomputed using a constant CO a priori profile,
22 which is 100.0 ppb in LMT (Supplemental Material Figure 1 and representative of clean air
23 conditions. When using common a priori profiles, both MOPITT and CrIS observations still
24 present a latitudinal pattern [Suppl. Figures 1 and 2] similar to the one shown in Fig. 3, which
25 indicates the consistency of measurements from two TIR sensors is insensitive to the choice
26 of a priori. The differences between CrIS and MOPITT TIR improved to 2.8 ppb (Suppl.
27 Table 1), showing similar measurement characteristics (sensitivity, accuracy, and precisions).
28 The mean and RMS of the differences between CrIS and MOPITT multi-spectral CO data
29 products are -23.6 ± 37.6 ppb (Table 3), which is greater than the differences between CrIS and
30 MOPITT TIR and also greater than the estimated measurement uncertainty. This difference is
31 expected between CrIS and MOPITT multispectral sensitivity as quantified by the averaging
32 kernels, which represent the sensitivity of the CO retrieval to the true state, as shown in Fig.



1 4A and Fig. 4B for CrIS and MOPITT, respectively. The higher amplitude averaging kernels
2 for MOPITT multi-spectral observations in Fig. 4B quantify the enhanced near surface
3 sensitivity.

4 **3.3 Characteristics of joint TROPOMI and CrIS CO profile observations**

5 To access the characteristics of improved tropospheric CO profiling when combining
6 TIR/NIR observations, we computed the averaging kernels, degrees of freedom for signal
7 (DOFS, the trace of averaging kernels), and error covariance matrix for both synergistic and
8 each instrument alone observations. We used the CrIS viewing geometry for the simulation of
9 TROPOMI measurements since the tandem orbit of Suomi NPP and TROPOMI is very
10 similar.

11 Figures 4-6 and Table 4 show the retrieval diagnostics. We find that the tropospheric CO
12 profiles generated from joint CrIS/TROPOMI measurements have vertical resolution (Fig.
13 4D), sensitivity (mean total DOFS of 2.22), and error characteristics (magenta lines in Fig. 6B
14 and 6C) similar to the MOPITT joint NIR/TIR measurements (Fig. 4A, Fig. 6A; Table 4,
15 mean total DOFS of 1.88). The synergistic CrIS/TROPOMI observations clearly distinguish
16 the LMT (green lines in Fig.4D) and middle troposphere (magenta lines in Fig. 4D). The
17 synergistic CrIS/TROPOMI measurements showed significant improvements on the
18 sensitivity in comparisons to individual measurements from both CrIS and TROPOMI
19 missions (Fig. 4B/C; Fig. 5; Table 4). The latitudinal gradient of biomass burning intensity
20 (Fig. 2F, Fig. 3C, fire counts 0-250; max fire radiative power 0-800 mW), CO concentration
21 (Fig. 3 A, 100-400 ppb), and the change of DOFS (Fig. 5, CrIS 1-1.7; TROPOMI 1-1.5) show
22 similar pattern across the transect. The synergistic CrIS/TROPOMI, however, had higher
23 DOFS, generally above 2.0, because of its higher LMT sensitivity (Table 4, DOFS of 0.9 for
24 joint vs. 0.6 for CrIS, TROPOMI alone). And the sensitivity of MOPITT TIR and CrIS
25 measurements for LMT are approximately identical (0.56 vs. 0.62). The estimated sensitivity
26 of joint CrIS/TROPOMI measurements show improvements in comparisons to MOPITT
27 synergistic TIR/NIR observations, possibly arise from TROPOMI is a ‘staring’ instrument,
28 which does not have the issue of geophysical radiance error found by Deeter et al. (2011) for
29 MOPITT NIR sensor that is a ‘dragging’ instrument. It is worth to note that the minimum
30 spectral SNR of TROPOMI measurements were used in synthetic TROPOMI alone and joint
31 CrIS/TROPOMI measurements, the actual performances of joint CrIS/TROPOMI could be
32 even better than that shown in Figs. 4-6.



1 The total error consists of two terms (Equation 5): the first term represents the smoothing
2 error and the second term is the measurement error. By incorporating radiances measured by
3 two nadir-viewing instruments (Equation 3), the error characteristics of joint CrIS/TROPOMI
4 tropospheric CO estimates can be substantially improved, in comparison with joint
5 CrIS/TROPOMI and each instrument alone. Particularly, in the altitude range from Surface to
6 3 km (~700 hPa), we have seen the total uncertainty reduced from 30% (using measurements
7 from each instrument alone) to 15% (joint TIR/NIR). This increased sensitivity and decrease
8 in uncertainty are critical for evaluating the role of tropical fires (or pyro-convection) on the
9 CO distribution (Fromm et al., 2005, 2006).

10

11 **4 Conclusions**

12 Based upon the MUSES synergistic retrieval algorithm, the combined CrIS/TROPOMI
13 observations can extend and improve on the EOS-Terra MOPITT multi-spectral carbon
14 monoxide profile data products with the higher vertical resolution and accuracy compared to
15 any single nadir-viewing platform and over 2.5 times higher spatial sampling than MOPITT.

16 The MUSES algorithm has been applied to retrieve carbon monoxide volume mixing ratio
17 profiles using full spectral resolution, single footprint CrIS measurements over Africa on
18 August 28, 2013. The agreement of retrieved carbon monoxide volume mixing ratio in the
19 lower most troposphere (surface to 3 km; ~700 hPa) between CrIS and MOPITT TIR data
20 products is -6.9 ± 22.8 ppb) when using different a priori profiles in retrievals; and 2.8 ± 24.9
21 ppb) when for using common a priori in retrievals.

22 The simulated synergistic retrievals of CrIS/TROPOMI yields 0.9 degrees of freedom for CO
23 signals in the LMT and 1.3 above LMT, distinguishing signals from the LMT and that above
24 LMT in the troposphere, similar to that of MOPITT multiple spectral observation (DOFS 0.8
25 in the LMT, and 1.1 above LMT). In addition to increased sensitivity, the joint retrievals
26 reduce measurement uncertainty, especially in the LMT, about 15% error reduction in the
27 altitude range from surface to 3 km (~700 hPa). The potentials of synergistic CrIS/TROPOMI
28 observations will be fully exploit using MUSES algorithm when TROPOMI Level 1B
29 spectral radiances become available (estimated in late 2016). The validation of CO retrievals
30 using aircraft in situ profiles will be accomplished in the near future.



1 By achieving information content that rivals the EOS-Terra MOPITT measurements,
2 synergistic CrIS/TROPOMI CO observations not only demonstrably enhances the scientific
3 value of S5p TROPOMI and Suomi NPP, but also extends the climate and tropospheric
4 records needed to continue NASA EOS science. Furthermore, the broad coverage of Suomi
5 NPP will provide global CO (a key tracer gas in the diagnostics of transport and chemical
6 reaction processes in the atmosphere) that compliments the NASA Decadal Survey GEO-
7 CAPE geostationary sounder (Fishman et al., 2012; <http://geo-cape.larc.nasa.gov/>). GEO-
8 CAPE is envisaged as a member of the Committee on Earth Observing Systems (CEOS) air
9 quality constellation, which includes the Korean GEMS (Bak et al., 2013), ESA Sentinel-4
10 (Ingmann et al., 2012; www.ceos.org/acc), and possibly Canadian PCW missions (Nassar et
11 al., 2014; <http://www.asc-csa.gc.ca/eng/satellites/pcw/>). The joint CrIS/TROPOMI retrieval
12 algorithm can also be applied to the future joint Sentinel-5 UVNS/IASI-NG observations
13 from METOP Second Generation satellites, which could provide joint NIR/TIR CO
14 measurements in the time period of 2022-2045 (Veefkind et al., 2012; Crevoisier et al., 2014).
15 The joint CrIS/TROPOMI CO profiles will enable the quantification of transport and
16 transformation of atmospheric composition in the domains unobserved by this constellation.
17 This combination of low-earth orbiting and geostationary space sounders would provide an
18 unprecedented atmospheric composition observing system needed to address long-term
19 scientific questions in climate, air quality, and atmospheric chemistry.

20

21 **Acknowledgements**

22 The authors thank Drs. Annmarie Eldering, Michael R. Gunson, Susan S. Kulawik, Karen
23 Cady-Pereira, Vivienne H. Payne, Bradley R. Pierce, and Stanley P. Sander for many helpful
24 discussions. Support from the NASA ROSE-2013 Atmospheric Composition: AURA Science
25 Team program (grant number: NNN13D455T) is gratefully acknowledged. Part of the
26 research was carried out at the Jet Propulsion Laboratory, California Institute of Technology,
27 under a contract with the National Aeronautics and Space Administration. Copyright 2015,
28 California Institute of Technology. Government sponsorship acknowledged.

29

30

31



1 **References**

- 2 Aumann H., Chahine M.T., Gautier C., Goldberg M.D, Kalnay E., McMillin L.M.,
3 Revercomb H., Rosenkranz P.W., Smith W.L., Staelin D.H., Strow L.L., and Susskind J.:
4 AIRS/AMSU/HSB on the Aqua mission: Design, science objectives, data products, and
5 processing systems, *IEEE Trans. Geosci. Remote Sensing*, 41, 253-264, 2003.
- 6 Bak J., Kim J.H., Liu X., Chance K., and Kim J.: Evaluation of ozone profile and tropospheric
7 ozone retrievals from GEMS and OMI spectra, *Atmos. Meas. Tech.*, 6, 239-249, 2013.
- 8 Baker N.: Joint Polar Satellite System (JPSS) VIIRS Cloud Cover/Layers Algorithm
9 Theoretical Basis Document (ATBD), NASA Goddard Space Flight Center Technical Report,
10 2011a.
- 11 Baker N.: Joint Polar Satellite System (JPSS) VIIRS Cloud Effective Particle Size and Cloud
12 Optical Thickness Algorithm Theoretical Basis Document (ATBD), NASA Goddard Space
13 Flight Center Technical Report, 2011b.
- 14 Baker N.: Joint Polar Satellite System (JPSS) Cloud Top Algorithm Theoretical Basis
15 Document (ATBD), NASA Goddard Space Flight Center Technical Report, 2012.
- 16 Boesch H., Brown L., Castano R., Christi M., Connor B., Crisp D., Eldering A., Fisher B.,
17 Frankenberg C., Gunson M., Granat R., McDuffie J., Miller C., Natraj V., O'Brien D., O'Dell
18 C., Osterman G., Oyafuso F., Payne V., Polonski I., Smyth M., Spurr R., Thompson D., Toon
19 G.: Orbiting Carbon Observatory-2 (OCO-2) Level 2 full physics retrieval algorithm
20 theoretical basis, version 2.0 revision 2, March 30 2015, data releases 6 and 6R.
21 http://disc.sci.gsfc.nasa.gov/OCO-2/documentation/oco-2-v6/OCO2_L2_ATBD.V6.pdf
- 22 Bowman K.W., Rodgers C.D., Kulawik S.S., Worden J., Sarkissian E., Osterman G., Steck
23 T., Lou M., Eldering A., Shephard M., Worden H., Lampel M., Clough S., Brown P.,
24 Rinsland C., Gunson M., Beer R.: Tropospheric Emission Spectrometer: Retrieval Method
25 and Error Analysis, *IEEE Trans. Geosci. Remote Sensing*, 44, 1297-1307, 2006.
- 26 Brasseur G.P., Hauglustaine D.A., Walters S., Rasch P.J., Muller J.F., Granier C., and Tie
27 X.X.: MOZART, a global chemical transport model for ozone and related chemical tracers 1.
28 Model description, *J. Geophys. Res.*, 103(D21), 28265-28289, 1998.
- 29 Buchard V., da Silva A. M., Colarco P. R., Darmenov A., Randles C. A., Govindaraju R.,
30 Torres O., Campbell J., and Spurr R.: Using the OMI aerosol index and absorption aerosol



- 1 optical depth to evaluate the NASA MERRA Aerosol Reanalysis, *Atmos. Chem. Phys.*, 15,
2 5743-5760, 2015.
- 3 Clerbaux C., Edwards D.P., Deeter M., Emmons L., Lamarque J.-F., Tie X.X., Massie S.T.,
4 and Gille J.: Carbon monoxide pollution from cities and urban areas observed by the
5 Terra/MOPITT mission, *Geophys. Res. Lett.*, 35, L03817, 1-6, 2008.
- 6 Clough S.A., Shephard M.W., Worden J., Brown P.D., Worden H.M., Luo M., Rodgers C.D.,
7 Rinsland C.P., Goldman A., Brown L., Kulawik S.S., Eldering A., Lampel M.C., Osterman
8 G., Beer R., Bowman K., Cady-Pereira K.E., Mlawer E.J.: Forward Model and Jacobians for
9 Tropospheric Emission Spectrometer Retrievals, *IEEE Trans. Geosci. Remote Sensing*, 44,
10 1308-1323, 2006.
- 11 Crevoisier C., Clerbaux C., Guidard V., Phulpin T., Armante R., Barret B., Camy-Peyret C.,
12 Chaboureaud J.-P., Coheur P.-F., Crépeau L., Dufour G., Labonnote L., Lavanant L., Hadji-
13 Lazaro J., Herbin H., Jacquinet-Husson N., Payan S., Péquignot E., Pierangelo C., Sellitto, P.,
14 and Stubenrauch C.: Towards IASI-New Generation (IASI-NG): impact of improved spectral
15 resolution and radiometric noise on the retrieval of thermodynamic, chemistry and climate
16 variables, *Atmos. Meas. Tech.*, 7, 4367-4385, 2014.
- 17 Cuesta J., Eremenko M., Liu X., Dufour G., Cai Z., Höpfner M., von Clarmann T., Sellitto P.,
18 Foret G., Gaubert B., Beekmann M., Orphal J., Chance K., Spurr R., and Flaud J.-M.:
19 Satellite observation of lowermost tropospheric ozone by multi- spectral synergism of IASI
20 thermal infrared and GOME-2 ultraviolet measurements, *Atmos. Chem. Phys.*, 13, 9675-9693
21 2013.
- 22 Davies D., Kumar S., and Descloitres J.: Global fire monitoring using MODIS near-real-time
23 satellite data, *GIM International*, 18(4): 41-43, 2004.
- 24 Deeter M.N., Worden H.M., Gille J.C., Edwards D.P., Mao D., and Drummond J.R.,
25 MOPITT multispectral CO retrievals: Origins and effects of geophysical radiance errors, *J.*
26 *Geophys. Res.*, 116, D15303, 2011.
- 27 Deeter M.N., Martínez-Alonso S., Edwards D.P., Emmons L.K., Gille J.C., Worden H.M.,
28 Pittman J.V., Daube B.C., and Wofsy S.C.: Validation of MOPITT Version 5 thermal-
29 infrared, near-infrared, and multispectral carbon monoxide profile retrievals for 2000–2011, *J.*
30 *Geophys. Res.*, 118(12), 6710-6725, 2013.



- 1 Deeter M.N., Martínez-Alonso S., Edwards D.P., Emmons L.K., Gille J.C., Worden H.M.,
2 Sweeney C., Pittman J.V., Daube B.C., and Wofsy S.C.: The MOPITT Version 6 product:
3 algorithm enhancements and validation, *Atmos. Meas. Tech.*, 7(11), 3623-3632, 2014.
- 4 de Laat A.T.J., Gloudermans A.M.S., Aben I., M. Krol, Meirink J.F., van der Werf G.R., and
5 Schrijver H.: Scanning Imaging Absorption Spectrometer for Atmospheric Chartography
6 carbon monoxide total columns: Statistical evaluation and comparison with chemistry
7 transport model results, *J. Geophys. Res.*, 112, D12310, 2007.
- 8 Drummond J.R.: Measurements of Pollution in the Troposphere (MOPITT), in *The Use of*
9 *EOS for Studies of Atmospheric Physics*, edited by J. C. Gille and G. Visconti, 77-101,
10 North-Holland, Amsterdam, 1992.
- 11 Edwards D.P., Emmons L.K., Gille J.C., Chu A., Attié J.-L., Giglio L., Wood S.W., Haywood
12 J., Deeter M.N., Massie S.T., Ziskin D.C. and Drummond J.R.: Satellite-observed pollution
13 from Southern Hemisphere biomass burning, *J. Geophys. Res.*, 111, D14312, 1-17, 2006.
- 14 Eldering A., Kulawik S.S., Worden J., Bowman K., and Osterman G.: Implementation of
15 cloud retrievals for TES atmospheric retrievals: 2. Characterization of cloud top pressure and
16 effective optical depth retrievals, *J. Geophys. Res.*, 113, D16S37, 2008.
- 17 Emmons L.K., Pfister G.G., Edwards D.P., Gille J.C., Sachse G., Blake D., Wofsy S., Gerbig
18 C., Matross D., and Nédélec P.: Measurements of pollution in the troposphere (MOPITT)
19 validation exercises during summer 2004 field campaigns over North America, *J. Geophys.*
20 *Res.*, 112, D12S02, 2007.
- 21 Emmons L.K., Edwards D.P., Deeter M.N., Gille J.C., Campos T., Nédélec P., Novelli P., and
22 Sachse G.: Measurements of Pollution in the Troposphere (MOPITT) validation through
23 2006, *Atmos. Chem. Phys.*, 9, 1795-1803, 2009.
- 24 Fishman J., Iraci L.T., Al-Saadi J., Chance K., Chavez F., Chin M., Coble P., Davis C.,
25 DiGiacomo P.M., Edwards D., Eldering A., Goes J., Herman J., Hu C., Jacob D. J., Jordan C.,
26 Kawa S.R., Key R., Liu X., Lohrenz S., Mannino A., Natraj V., Neil D., Neu J., Newchurch
27 M., Pickering K., Salisbury J., Sosik H., Subramaniam A., Tzortziou M., Wang J., and Wang
28 M.: The United States' Next Generation of Atmospheric Composition and Coastal Ecosystem
29 Measurements: NASA's Geostationary Coastal and Air Pollution Events (GEO-CAPE)
30 Mission. *Bull. Amer. Meteor. Soc.*, 93, 1547-1566, 2012.



- 1 Fortems-Cheiney A., Chevallier F., Pison I., Bousquet P., Szopa S., Deeter M.N., and
2 Clerbaux C.: Ten years of CO emissions as seen from Measurements of Pollution in the
3 Troposphere (MOPITT), *J. Geophys. Res.*, 116, D05304, 1-17, 2011.
- 4 Fromm M., Bevilacqua R., Servranckx R., Rosen J., Thayer J.P., Herman J., and Larko D.:
5 Pyro-cumulonimbus injection of smoke to the stratosphere: Observations and impact of a
6 super blowup in northwestern Canada on 3–4 August 1998, *J. Geophys. Res.*, 110, D08205,
7 2005.
- 8 Fromm M., Tupper A., Rosenfeld D., Servranckx R., and McRae R.: Violent pyro-convective
9 storm devastates Australia’s capital and pollutes the stratosphere, *Geophys. Res. Lett.*, 33,
10 L05815, 2006.
- 11 Fu D., Worden J.R., Liu X., Kulawik S.S., Bowman K.W., and Natraj V.: Characterization of
12 ozone profiles derived from Aura TES and OMI radiances, *Atmos. Chem. Phys.*, 13, 3445-
13 3462, 2013.
- 14 Gambacorta A., Barnet C., Wolf W., King T., Maddy E., Strow L., Xiong X., Nalli N., and
15 Goldberg M.: An Experiment Using high spectral resolution CrIS measurements for
16 atmospheric trace gases: carbon monoxide retrieval impact study, *IEEE Geoscience and
17 Remote Sensing Letters*, 11, 9, 1639-1643, 2014.
- 18 George M., Clerbaux C., Hurtmans D., Turquety S., Coheur P.-F., Pommier M., Hadji-Lazaro
19 J., Edwards D.P., Worden H., Luo M., Rinsland C., and McMillan W.: Carbon monoxide
20 distributions from the IASI/ METOP mission: Evaluation with other space-borne remote
21 sensors, *Atmos. Chem. Phys.*, 9, 8317-8330, 2009.
- 22 Giglio L., Descloitres J., Justice C.O., and Kaufman Y.J.: An enhanced contextual fire
23 detection algorithm for MODIS, *Remote Sensing of Environment*, 87, 273-282, 2003.
- 24 Han Y., Revercomb H., Crompton M., Gu D., Johnson D., Mooney D., Scott D., Strow L.,
25 Bingham G., Borg L., Chen C., DeSlover D., Esplin M., Hagan D., Jin X., Knuteson R.,
26 Motteler H., Predina J., Suwinski L., Taylor J., Tobin D., Tremblay D., Wang C., Wang L.,
27 Wang L., Zavyalov V.: Suomi NPP CrIS measurements, sensor data record algorithm,
28 calibration and validation activities, and record data quality, *J. Geophys. Res. Atmos.*, 118,
29 12734-12748, 2013.
- 30 Han Y., Chen Y., Xiong X., and Jin X.: S-NPP CrIS full spectral resolution SDR processing
31 and data quality assessment, 95th AMS Annual Meeting, Phoenix, Arizona, January 2015.



- 1 Heald C.L., Jacob D.J., Fiore A.M., Emmons L.K., Gille J.C., Deeter M.N., Warner J.,
2 Edwards D.P., Crawford J.H., Hamlin A.J., Sachse G.W., Browell E.V., Avery M.A., Vay
3 S.A., Westberg D.J., Blake D.R., Singh H.B., Sandholm S.T., Talbot R.W., and Fuelberg
4 H.E.: Asian outflow and trans-Pacific transport of carbon monoxide and ozone pollution: An
5 integrated satellite, aircraft, and model perspective, *J. Geophys. Res.*, 108(D24), 4804-4820,
6 2003.
- 7 Hook S., Friedl M., Sulla-Menashe D., Gray J., Schaaf C., Wang Z., Miura T., Huete A.,
8 Maslanik J., Tschudi M., Baldwin D., Key J.R., Wang X., Liu Y., Riggs G., Hall D., Ellicott
9 E., Giglio L., Schroeder W., Csiszar I., Lyapustin A., Vermote E., Wang Y., Myneni R.,
10 Wolfe R., Foster J., Masuoka E.J., Devadiga S., Davidson C.: An Evaluation of the Suomi-
11 NPP Visible Infrared Imaging Radiometer Suite (VIIRS) and the Associated Environmental
12 Data Records for Land Science after Early Evaluation on On-Orbit Performance, NASA
13 Goddard Space Flight Center Technical Report, 2012.
- 14 Ingmann P., Veihelmann B., Langen J., Lamarre D., Stark H., Bazalgette G. Lacoste C.:
15 Requirements for the GMES Atmosphere Service and ESA's implementation concept:
16 Sentinels-4/-5 and -5p, *Remote Sensing of Environment*, 120, 58-69, 2012.
- 17 Kalnay E., Kanamitsu M., Kistler R., Collins W., Deaven D., Gandin L., Iredell M., Saha S.,
18 White G., Woollen J., Zhu Y., Chelliah M., Ebisuzaki W., Higgins W., Janowiak J., Mo K.C.,
19 Ropelewski C., Wang J., Leetmaa A., Reynolds R., Jenne R., and Joseph D.: The
20 NCEP/NCAR 40-year reanalysis project, *B. Am. Meteorol. Soc.*, 77(3), 437-471, 1996.
- 21 Kar J., Deeter M.N., Fishman J., Liu Z., Omar A., Creilson J. K., Trepte C.R., Vaughan M.A.,
22 and Winker D.M.: Wintertime pollution over the eastern Indo-Gangetic Plains as observed
23 from MOPITT, CALIPSO and tropospheric ozone residual data, *Atmos. Chem. Phys.*, 10,
24 12273-12283, 2010.
- 25 Kopacz M., Jacob D.J., Henze D.K., Heald C.L., Streets D.G., and Zhang Q.: Comparison of
26 adjoint and analytical Bayesian inversion methods for constraining Asian sources of carbon
27 monoxide using satellite (MOPITT) measurements of CO columns, *J. Geophys. Res.*, 114,
28 D04305, 1-10, 2009.
- 29 Kulawik S.S., Worden J., Eldering A., Bowman K., Gunson M., Osterman G.B., Zhang L.,
30 Clough S., Shephard M.W., and Beer R.: Implementation of cloud retrievals for Tropospheric



- 1 Emission Spectrometer (TES) atmospheric retrievals: part 1. Description and characterization
- 2 of errors on trace gas retrievals, *J. Geophys. Res.*, 111, D24204, 2006.
- 3 Landgraf J. and Hasekamp O.P.: Retrieval of tropospheric ozone: The synergistic use of
- 4 thermal infrared emission and ultraviolet reflectivity measurements from space, *J. Geophys.*
- 5 *Res.*, 112, D08310, 2007.
- 6 McMillan W.W., Barnet C., Strow L., Chahine M.T., McCourt M.L., Warner J.X., Novelli
- 7 P.C., Korontzi S., Maddy E.S., and Datta S.: Daily global maps of carbon monoxide from
- 8 NASA's Atmospheric Infrared Sounder, *Geophys. Res. Lett.*, 32, L11801, 1 – 4, 2005.
- 9 Nassar R., Sioris C.E., Jones D.B.A., and McConnell J.C.: Satellite observations of CO₂ from
- 10 a highly elliptical orbit for studies of the Arctic and boreal carbon cycle, *J. Geophys. Res.*
- 11 *Atmos.*, 119, 2654-2673, 2014.
- 12 Pagano T.S., Aumann H.H., Hagan D.E., and Overoye K.: Prelaunch and in-flight radiometric
- 13 calibration of the Atmospheric Infrared Sounder (AIRS), *Geoscience and Remote Sensing,*
- 14 *IEEE Transactions on*, 41(2), 265-273, 2003.
- 15 Park M., Randel W.J., Kinnison D.E., Garcia R.R., and Choi W.: Seasonal variation of
- 16 methane, water vapor, and nitrogen oxides near the tropopause: Satellite observations and
- 17 model simulations, *J. Geophys. Res., Atmos.*, 109, D03302, 2004.
- 18 Platnick S, Ackerman S.A., Baum B.A., Heidinger A.K., Holz R.E., King M.D., Menzel
- 19 W.P., Nasiri S., Weisz E., Yang P.: Assessment of IDPS VIIRS Cloud Products and
- 20 Recommendations for EOS-ERA Cloud Climate Data Record Continuity, NASA Goddard
- 21 Space Flight Center Technical Report, 2013.
- 22 Rienecker M., Suarez M.J., Todling R., Bacmeister J., Takacs L., Liu H.-C., Gu W.,
- 23 Sienkiewicz M., Koster R. D., Gelaro R., Stajner I., and Nielsen J. E.: The GEOS-5 data
- 24 assimilation system-documentation of versions 5.0.1, 5.1.0, and 5.2.0., technical report series
- 25 on global modeling and data assimilation, 104606, 27, 2008.
- 26 Rienecker M.M., Suarez M.J., Gelaro R., Todling R., Bacmeister J., Liu E., Bosilovich M.G.,
- 27 Schubert S.D., Takacs L., Kim G.-K., Bloom S., Chen J., Collins D., Conaty A., da Silva A.,
- 28 Gu W., Joiner J., Koster R.D., Lucchesi R., Molod A., Owens T., Pawson S., Pegion P.,
- 29 Redder C.R., Reichle R., Robertson F.R., Ruddick A.G., Sienkiewicz M., and Woollen J.:
- 30 MERRA: NASA's Modern-Era Retrospective Analysis for Research and Applications. *J.*
- 31 *Climate*, 24, 3624-3648, 2011.



- 1 Rinsland C.P., Luo M., Logan J.A., Beer R., Worden H., Kulawik S.S., Rider D., Osterman
2 G., Gunson M., Eldering A., Goldman A., Shephard M., Clough S.A., Rodgers C., Lampel M.
3 and Chiou L.: Nadir measurements of carbon monoxide distributions by the Tropospheric
4 Emission Spectrometer instrument onboard the Aura Spacecraft: Overview of analysis
5 approach and examples of initial results, *Geophys. Res. Lett.*, 33, L22806, 2006.
- 6 Rodgers C.D.: *Inverse methods for atmospheric sounding: Theory and practice*, World
7 Scientific Publishing, Singapore, 2000.
- 8 Seemann S.W., Borbas E.E., Knuteson R.O., Stephenson G.R., and Huang H.-L.:
9 Development of a global infrared land surface emissivity database for application to clear sky
10 sounding retrievals from multispectral satellite radiance measurements. *J. Appl. Meteor.*
11 *Climatol.*, 47, 108-123, 2008.
- 12 Shindell D.T., Faluvegi G., Stevenson D.S., Krol M.C., Emmons L.K., Lamarque J.-F., Pétron
13 G., Dentener F.J., Ellingsen K., Schultz M.G., Wild O., Amann M., Atherton C.S., Bergmann
14 D.J., Bey I., Butler T., Cofala J., Collins W.J., Derwent R.G., Doherty R.M., Drevet J., Eskes
15 H.J., Fiore A.M., Gauss M., Hauglustaine D.A., Horowitz L.W., Isaksen I.S.A., Lawrence
16 M.G., Montanaro V., Müller J.-F., Pitari G., Prather M.J., Pyle J.A., Rast S., Rodriguez J.M.,
17 Sanderson M.G., Savage N.H., Strahan S.E., Sudo K., S. Szopa, Unger N., van Noije T.P.C.
18 and Zeng G.: Multimodel simulations of carbon monoxide: Comparison with observations
19 and projected near-future changes, *J. Geophys. Res.*, 111, D19306, 1-24, 2006.
- 20 Silva S.J., Arellano A.F., and Worden H.M.: Toward anthropogenic combustion emission
21 constraints from space-based analysis of urban CO₂/CO sensitivity, *Geophys. Res. Lett.*,
22 40(18), 4971-4976, 2013.
- 23 Spurr R.J.D.: VLIDORT: A linearized pseudo-spherical vector discrete ordinate radiative
24 transfer code for forward model and retrieval studies in multilayer multiple scattering media,
25 *J. Quant. Spectrosc. and Radiat. Transfer*, 102(2): 316-342, 2006.
- 26 Spurr R.J.D., de Haan J., van Oss R., and Vasilkov A.: Discrete Ordinate Theory in a
27 Stratified Medium with First Order Rotational Raman Scattering: a General Quasi-Analytic
28 Solution, *J. Quant. Spectrosc. Radiat. Transfer*, 109, 404-425, 2008.
- 29 Strow L., Blackwell W., Fishbein E., Lambrigtsen B., and Revercomb H.: NPP Sounding
30 Group Evaluation Report, NASA Goddard Space Flight Center Technical Report, 2013a.



- 1 Strow, L. L., Motteler H., Tobin D., Revercomb H., Hannon S., Buijs H., Predina J., Suwinski
2 L., and Glumb R.: Spectral calibration and validation of the Cross-track Infrared Sounder on
3 the Suomi NPP satellite, *J. Geophys. Res. Atmos.*, 118, 12486-12496, 2013b.
- 4 Tobin D., Revercomb H., Knuteson R., Taylor J., Best F., Borg L., DeSlover D., Martin G.,
5 Buijs H., Esplin M., Glumb R., Han Y., Mooney D., Predina J., Strow L., Suwinski L., Wang
6 L.: Suomi-NPP CrIS radiometric calibration uncertainty, *J. Geophys. Res. Atmos.*, 118,
7 10589-10600, 2013.
- 8 Veefkind J.P., Aben I., McMullan K., Försterd H., de Vries J., Otter G., Claas J., Eskes H.J.,
9 de Haan J.F., Kleipool Q., van Weele M., Hasekamp O., Hoogeveen R., Landgraf J., Snel R.,
10 Tol P., Ingmann P., Voors R., Kruizinga B., Vink R., Visser H., Levelt P.F.: TROPOMI on
11 the ESA Sentinel-5 Precursor: A GMES mission for global observations of the atmospheric
12 composition for climate, air quality and ozone layer applications, *Remote Sensing of*
13 *Environment*, 120, 70-83, 2012.
- 14 Wang L., Tremblay D.A., Han Y., Esplin M., Hagan D.E., Predina J., Suwinski L., Jin X., and
15 Chen Y.: Geolocation assessment for CrIS sensor data records, *J. Geophys. Res. Atmos.*, 118,
16 12690-12704, 2013.
- 17 Warner J., Comer M.M., Barnet C.D., McMillan W.W., Wolf W., Maddy E., and Sachse G.:
18 A comparison of satellite tropospheric carbon monoxide measurements from AIRS and
19 MOPITT during INTEX-A, *J. Geophys. Res.*, 112, D12S17, 1-18, 2007.
- 20 Worden H.M., Deeter M.N., Edwards D.P., Gille J.C., Drummond J.R., and Nédélec P.P.:
21 Observations of near-surface carbon monoxide from space using MOPITT multispectral
22 retrievals, *J. Geophys. Res.*, 115, D18314, 2010.
- 23 Worden H.M., Deeter M.N., Frankenberg C., George M., Nichitiu F., Worden J., Aben I.,
24 Bowman K.W., Clerbaux C., Coheur P.F., de Laat A.T.J., Detweiler R., Drummond J.R.,
25 Edwards D.P., Gille J.C., Hurtmans D., Luo M., Martínez-Alonso S., Massie S., Pfister G.,
26 and Warner J.X.: Decadal record of satellite carbon monoxide observations, *Atmos. Chem.*
27 *and Phys.*, 13, 837-850, 2013a.
- 28 Worden H.M., Edwards D.P., Deeter M.N., Fu D., Kulawik S.S., Worden J.R., and Arellano
29 A.: Averaging kernel prediction from atmospheric and surface state parameters based on
30 multiple regression with MOPITT CO and TES-OMI O₃ multispectral observations, *Atmos.*
31 *Meas. Tech.*, 6, 1633-646, 2013b.



1 Zhang L., Jacob D.J., Bowman K.W., Logan J.A., Turquety S., Hudman R.C., Li Q., Beer R.,
2 Worden H.M., Worden J.R., Rinsland C.P., Kulawik S.S., Lampel M.C., Shephard M.W.,
3 Fisher B.M., Eldering A., and Avery M.A.: Ozone-CO correlations determined by the TES
4 satellite instrument in continental outflow regions, *Geophys. Res. Lett.*, 33, 2006.

5

6

7

8

9

10

11

12

13

14

15

16

17

18

19

20

21

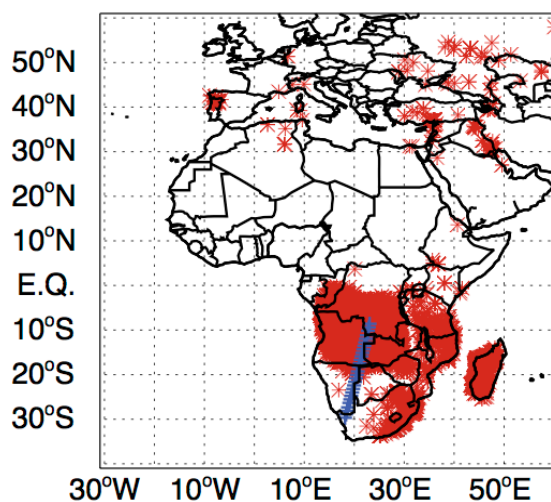
22

23

24

25

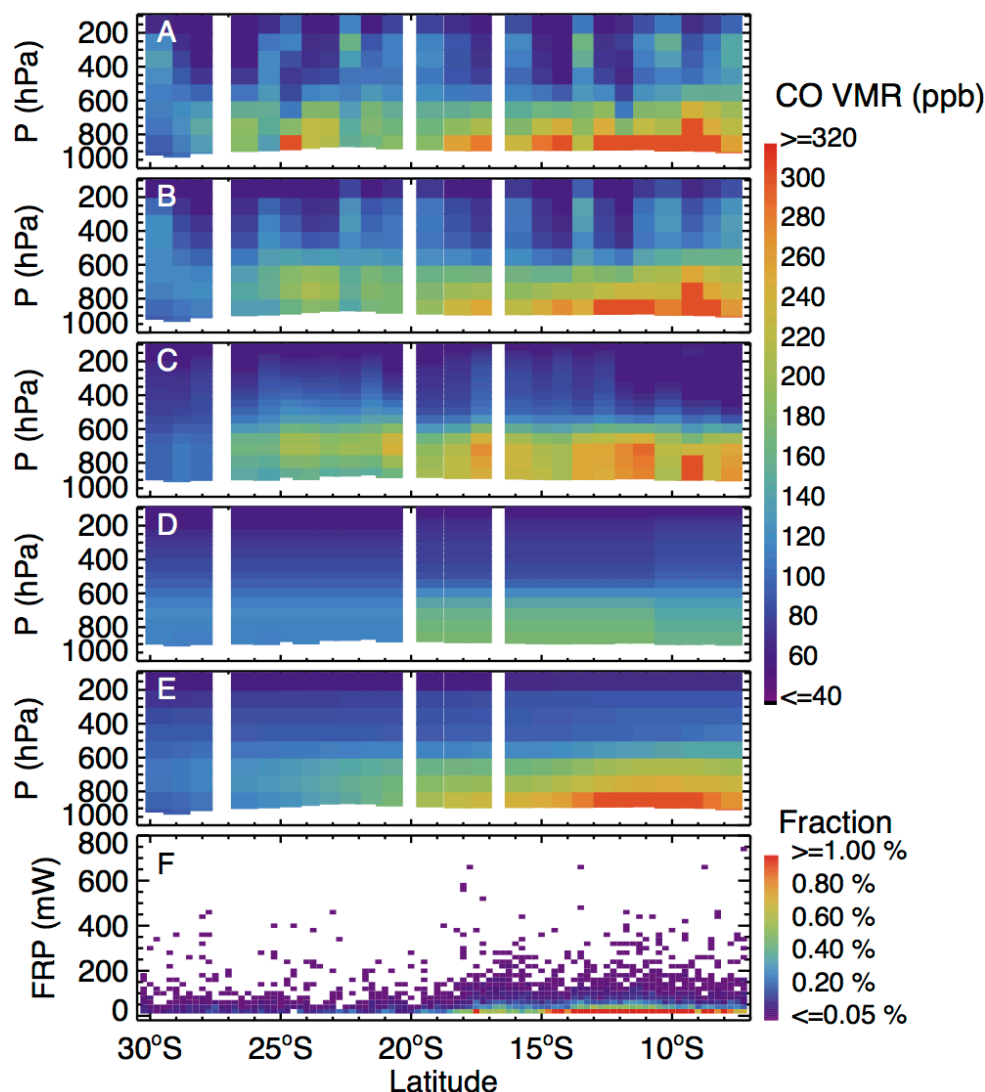
26



1

2 **Figure 1.** Collocated Suomi-NPP CrIS measurements (blue cross) over Africa on August 28th,
3 2013 and Terra MOPITT observations on August 27th, 2013. The red stars represent the fire
4 location measured by Aqua MODIS on August 28th, 2013.

5



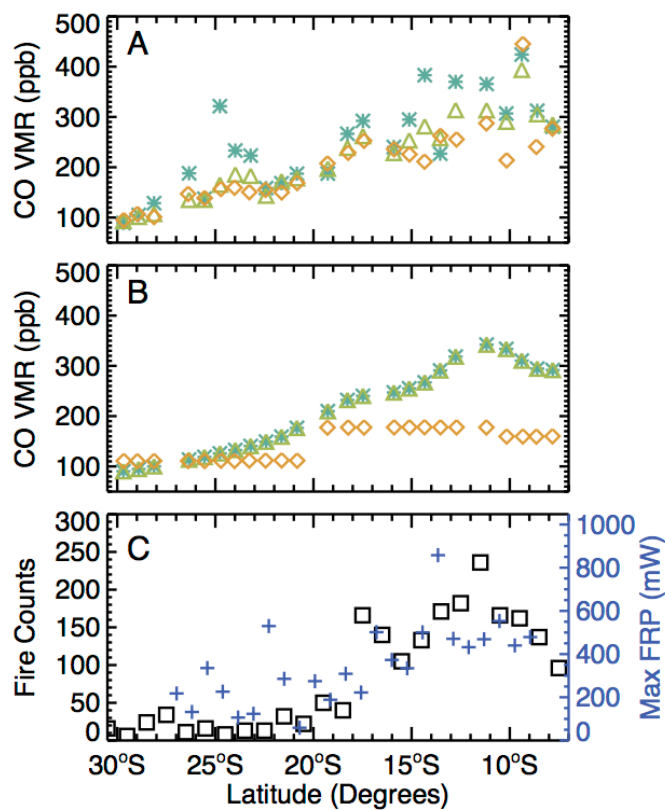
1

2 **Figure 2.** Tropospheric carbon monoxide (CO) volume mixing ratio (parts-per-billion)
3 profiles measured by Terra MOPITT (version 6.0) on August 27th, Suomi-NPP CrIS on
4 August 28th 2013, and fire radiative power (milliwatts) measured by Aqua MODIS. (Panel A)
5 MOPITT multiple spectral CO fields; (Panel B) MOPITT thermal infrared CO fields; (Panel
6 C) CrIS thermal infrared CO fields using a priori profiles identical to those used in the Aura
7 TES operational retrievals; (Panel D) a priori CO fields used in CrIS retrievals shown in Panel
8 C. (Panel E) a priori profiles identical to those used in the MOPITT operational retrievals
9 shown in Panels A and B; (Panel F) Fire radiative power measured by Aqua MODIS over
10 Africa for August 28th, 2013.

11
12



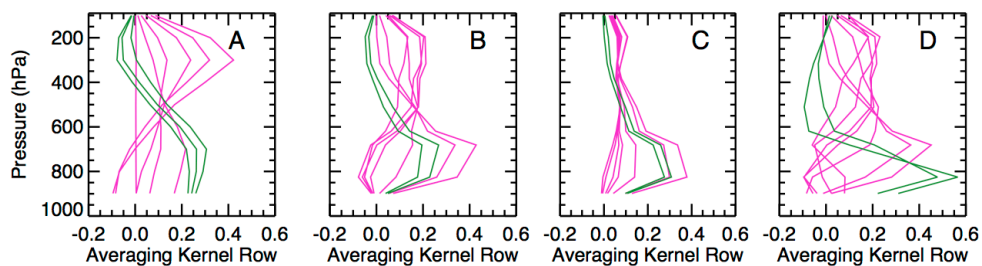
1
2
3



4

5 **Figure 3.** Averaged carbon monoxide (CO) volume mixing ratio (parts-per-billion) from
6 surface to 3km (~700-hPa), fire counts and maximum fire radiative power (milliwatts)
7 measured by Aqua MODIS over Africa for August 28th, 2013. (Panel A) MOPITT multiple
8 spectral CO data products (blue stars), MOPITT thermal infrared CO data products (green
9 triangles), and CrIS thermal infrared CO VMR using a priori profiles identical to those used
10 in the Aura TES operational retrievals (golden diamonds); (Panel B) a priori CO VMR used
11 in MOPITT (green/blue) and CrIS (gold) retrievals. (Panel C) Fire counts (black squares) and
12 maximum fire radiative power (blue plus) among the Auqa MODIS measurements whose data
13 quality confidences are greater than 70%.

14
15
16
17
18
19



1

2 **Figure 4.** Sample averaging kernels of measurements for the target scene near 22.99°E,
3 8.65°S. In all panels, green lines are the averaging kernels from the surface to 3 km (~700
4 hPa); magenta lines are the averaging kernels from 3 km (~700 hPa) to 100 hPa. (Panel A)
5 MOPITT joint NIR/TIR measurements; (Panel B) Suomi-NPP CrIS measurements; (Panel C)
6 synthetic S5p TROPOMI measurements; (Panel D) synthetic joint TROPOMI/CrIS
7 measurements.

8

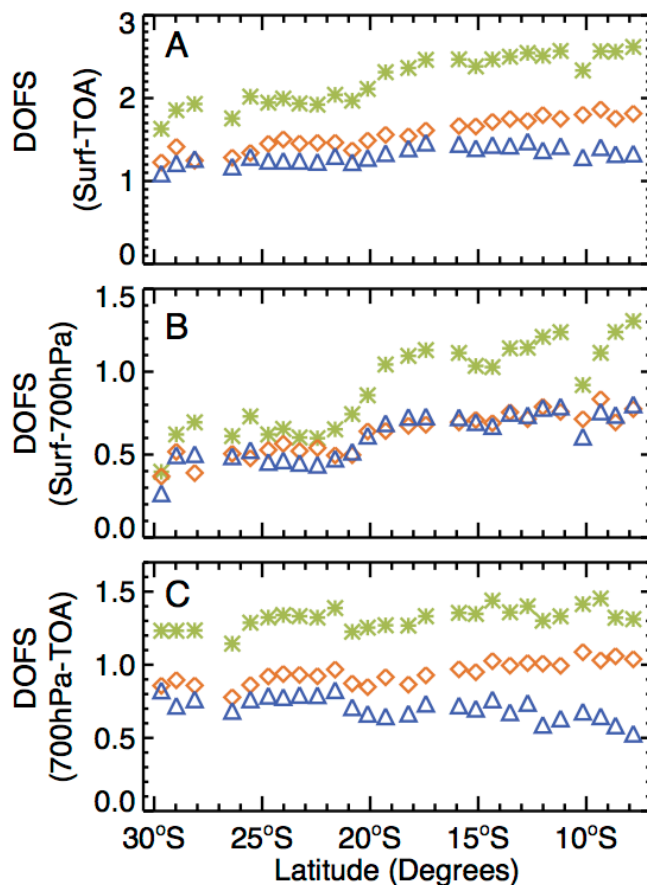
9

10

11

12

13



1

2 **Figure 5.** Degrees of freedom for CO measurements from CrIS, along with the synthetic
3 TROPOMI alone and joint CrIS and TROPOMI measurements over the biomass-burning
4 region. Green stars are the DOFS for joint TROPOMI and CrIS; gold diamonds are for the
5 DOFS for CrIS; and blue triangles are for DOFS from TROPOMI measurements.

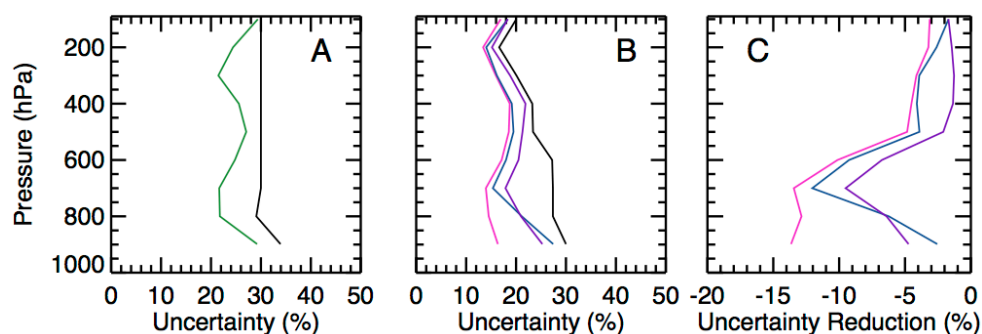
6

7

8

9

10



1

2 **Figure 6.** Uncertainties of the carbon monoxide (CO) volume mixing ratio (VMR) profiles
3 near 22.99°E, 8.65°S on August 28th, 2013. (Panel A) Uncertainty of the joint MOPITT
4 multiple spectral CO products (green line), and a priori profile (black line); (Panel B)
5 Uncertainty of CrIS actual CO measurements (blue line), synthetic TROPOMI (purple line)
6 and joint CrIS/TROPOMI (magenta line) CO measurements. Black line is the uncertainty of a
7 priori profile used in the retrievals; (Panel C) The reduction on the uncertainty with respect to
8 the uncertainty of a priori profile.

9

10

11

12

13

14

15

16

17

18

19

20

21

22

23

24

25

26

27

28

29



1 **Table 1.** Satellite missions that measure tropospheric carbon monoxide.

Mission	Nominal	Years after Its	Spectral Resolution		Footprint	Swath
	Life Time	Design Life Time	cm ⁻¹		Size	Width
	Start – End	Year	TIR ^A	NIR ^B	km ²	km
CrIS/TROPOMI	2016 – 2023	0	0.625 ^C	0.458	14 × 14 ^D	2200
MOPITT	2000 – 2006	9	~0.04 eff ^E	~0.25 eff ^E	22 × 22	640
CrIS	2011 – 2026	0	0.625 ^C	NA	π × 441 ^{D,F}	2200
TES	2004 – 2010	5	0.060 ^C	NA	8 × 5	5
AIRS	2002 – 2008	7	~ 1.800	NA	π × 441 ^{D,F}	1600
TROPOMI	2016 – 2023	0	NA	~ 0.458	7 × 7	2600
SCIAMACHY	2002 – 2007	Terminated ^G	NA	~ 0.485	30 × 120	960

2 ^A First fundamental band of carbon monoxide, centered around 4.6 μm in the thermal infrared.

3 ^B First overtone band of carbon monoxide, centered around 2.3 μm in the near infrared.

4 ^C Specified values are the spectral resolution without apodization.

5 ^D The spatial resolution of data products from this work are 9 times higher than the existing operational CrIS and AIRS data products, since we use single footprint CrIS

6 L1B radiances in the retrievals, instead of cloud cleared radiances.

7 ^E MOPITT uses gas filter correlation radiometry (GFCR) with estimated effective spectral resolution.

8 ^F Estimated footprint sizes of AIRS and CrIS measurements since both sensors have circular fields of view.

9 ^G The measurements from SCIAMACHY ceased in 2012.

10

11

12

13

14

1 **Table 2.** List of parameters in state vector.

Case Selection ^A	Fitting Parameters	Number of Parameters	A Priori	A Priori Uncertainty
CrIS/TROPOMI, CrIS, TROPOMI	CO at each pressure level	14	MOZART-3 ^B	MOZART-3
CrIS/TROPOMI, CrIS, TROPOMI	H ₂ O at each pressure level	16	GEOS-5 ^C	NCEP ~30% ^D
CrIS/TROPOMI, CrIS	N ₂ O at each pressure level	25	MOZART-3	MOZART-3
CrIS/TROPOMI, CrIS, TROPOMI	CH ₄ at each pressure level	25	MOZART-3	MOZART-3
CrIS/TROPOMI, CrIS	Surface temperature	1	GEOS-5	0.5K
CrIS/TROPOMI, CrIS	Surface emissivity ^E	5	UOW-M data base ^F	~0.006
CrIS/TROPOMI, CrIS	Cloud extinction ^G	3	Initial BT difference	300%
CrIS/TROPOMI, CrIS	Cloud top pressure ^G	1	500 mbar	100%
CrIS/TROPOMI, TROPOMI	Gaussian parameters of optical depth profile for ice cloud ^H	3	[0.0125,0.30,0.04] ^I	[7.4,0.2,0.01] ^I
CrIS/TROPOMI, TROPOMI	Gaussian parameters of optical depth profile for water cloud ^H	3	[0.0125,0.75,0.10] ^I	[7.4,0.4,0.01] ^I
CrIS/TROPOMI, TROPOMI	Gaussian parameters of optical depth profile for primary aerosols ^H	3	[MERRA ^J ,0.90,0.05] ^I	[7.4,0.4,0.01] ^I
CrIS/TROPOMI, TROPOMI	Gaussian parameters of optical depth profile for secondary aerosols ^H	3	[MERRA ^J ,0.90,0.05] ^I	[7.4,0.4,0.01] ^I
CrIS/TROPOMI, TROPOMI	Surface albedo zero order term	1	from Spectra ^K	0.2
CrIS/TROPOMI, TROPOMI	Surface albedo first order term	1	0	0.0005/cm ⁻¹
CrIS/TROPOMI, TROPOMI	Radiance/irradiance wavelength shifts	2	0	0.5 cm ⁻¹

2 ^A The parameters are included in the retrievals for different cases (CrIS only, TROPOMI only, and joint CrIS/TROPOMI)3 ^B Model for Ozone and Related chemical Tracers (MOZART) 3 (Brasseur et al. 1998; Park et al. 2004)4 ^C Goddard Earth Observing System, version 5 (GEOS-5) (Rienecker et al., 2008)5 ^D National Center for Environmental Prediction (NCEP) reanalysis (Kalnay et al., 1996)6 ^E Retrievals over land, spectral surface emissivity is included.7 ^F Global infrared land surface emissivity database at University of Wisconsin-Madison (UOW-M) (Seemann et al., 2008).8 ^G For cloud treatment in TIR spectral region, we adopt the approach used in the TES Level 2 full physics retrieval algorithm (Kulawik et al., 2006; Eldering et al., 2008).9 ^H For cloud treatment in NIR spectral region, we adopt the approach used in the OCO-2 Level 2 full physics retrieval algorithm (Pages 28-31, 44-45, Boesch et al., 2015).
10 The wavelength-dependent optical property would be scaled to that of TROPOMI.11 ^I Gaussian parameters represent the total optical depth, peak altitude, and profile width. The peak altitude and profile width are normalized to the pressure at surface.12 ^J Modern Era Retrospective analysis for Research and Applications aerosol reanalysis (MERRAero) climatology (2009-2010) (Rienecker et al., 2011; Buchard et al., 2015)13 ^K The surface is assumed to be Lambertian with a variable slope in wavelength to the albedo, such that the albedo can vary linearly across the spectral band. A priori value
14 of surface albedo for zero order term are estimated from the measured continuum radiances, using the following equation: $A = \frac{\pi I}{\mu_0 I_0}$, where, I is the measured earth shine
15 radiance in the continuum, I₀ is the solar continuum spectral irradiance, μ₀ is the cosine of the solar zenith angle.



1 **Table 3.** The differences of carbon monoxide volume mixing ratio in the lower troposphere (surface to 3km (~700 hPa)) between CrIS and
2 MOPITT measurements shown in Figure 3A.

Data Product	Mean	RMS
	ppb	ppb
CrIS - MOPITT TIR	-6.9	22.8
CrIS - MOPITT Joint TIR/NIR	-22.9	38.8

3

4

5

6

7

8

9

10

11

12



1 **Table 4.** Degree of freedom for MOPITT, CrIS, and TROPOMI carbon monoxide measurements.

Altitude Range	Sensor	TIR	NIR	Joint TIR/NIR
Surface to Top of Atmosphere	MOPITT	1.44	0.51	1.88
	CrIS	1.57	-	2.22
	TROPOMI	-	1.32	
Surface to 3 km (~700 hPa)	MOPITT	0.56	0.30	0.77
	CrIS	0.62	-	0.91
	TROPOMI	-	0.61	
3 km (~700 hPa) to Top of Atmosphere	MOPITT	0.89	0.21	1.11
	CrIS	0.94	-	1.32
	TROPOMI	-	0.71	

2
 3
 4
 5
 6
 7
 8
 9
 10
 11